SCIENCE CHINA
Earth Sciences

• RESEARCH PAPER •

February 2016 Vol.59 No.2: 371–383
doi: 10.1007/s11430-015-5204-5

Numerical evaluation of the shear stimulation effect in naturally fractured formations

WANG Yu[1], LI Xiao[1*], ZHOU RunQing[1] & TANG ChunAn[2]

[1] *Key Laboratory of Shale Gas and Geoengineering, Institute of Geology and Geophysics, Chinese Academy of Sciences, Beijing 100029, China;*
[2] *School of Civil and Hydraulic Engineering, Dalian University of Technology, Dalian 116024, China*

Received May 26, 2015; accepted August 22, 2015; published online November 13, 2015

Abstract In shale gas fracking, the stimulated natural fracture system is often critical to the gas production. In this paper, we present the results of state-of-the-art modeling of a detailed parametric evolution of the shear stimulation effect in discrete fracture network (DFN) formations. Two-dimensional computational modeling studies have been used in an attempt towards understanding how naturally fractured reservoirs response in hydraulic fracturing. Simulations were conducted as a function of: (1) the *in-situ* stress ratio; (2) internal friction angle of DFN; (3) DFN orientation with the stress field; and (4) operational variables such as injection rate. A sensitivity study reveals a number of interesting observations resulting from these parameters on the shear stimulation in natural fracture system. This work strongly links the production technology, geomechanical evaluation and aids in the understanding and optimization of hydraulic fracturing simulations in naturally fractured reservoirs.

Keywords Hydraulic fracturing, DFN, Numerical simulation, Shear stimulation effect

Citation: Wang Y, Li X, Zhou R Q, Tang C A. 2016. Numerical evaluation of the shear stimulation effect in naturally fractured formations. Sci China Earth Sci, 59: 371−383, doi: 10.1007/s11430-015-5204-5

1. Introduction

Due to the low permeability of many shale reservoirs, a combined application of two technologies, horizontal drilling and massive multi-stage hydraulic fracturing (MMHF) has made vast resources of shale gas commercially viable (Gale and Holder, 2008; Jeffrey et al., 2010; King, 2010). The MMHF is a key well-established reservoir stimulation technique, which has been developed over the last half century. In shale gas fracturing, micro-seismic observations have illuminated a complex internal structure resulting from the interaction between the induced hydraulic fractures and natural fractures. It is widely speculated that the stimulated natural fractures can make a significant contribution to the gas production. In ultra-tight reservoirs such as shales, the connected reservoir conductivity is created in the process of hydraulic fracturing and that enables any measurable hydrocarbon production. The key to shale gas production is the presence of natural fractures (Palmer and Moschovidis, 2010; Chong et al., 2010) and planes of weakness that can result in complex fracture geometries during stimulations. The very productive wells were attributed to the stimulation of the natural fractures (Cipolla et al., 2009a, 2009b; Warpinski et al., 2009). This explanation was further supported by the interpretations of the micro-seismic date (Mayerhofer et al., 2006, 2010). Furthermore, the fracture aperture, abundance, connectivity, intersection, etc., and how difficult they can be opened and maintain flow in both primary and secondary natural fractures systems are critical to shale gas production. If so, the completion engineers need tools to design simulations that can address both the

*Corresponding author (email: lixiao@mail.iggcas.ac.cn)

geomechanics of creating hydraulic fractures and the geomechanics of the natural fracture system. Naturally sealed fracture systems reactivate during stimulation and their efficiency is enhanced by widening the treatment zone. So understanding the development and stimulation of the natural fracture system is often significant to an economically successful well.

The numerical tools used to simulate the naturally fractured formations could be roughly divided into three kinds. The first kind is the traditional finite element approach. Rahaman et al. (2009) and Nassir et al. (2010) have attempted to model the complex interactions of a created hydraulic fracture with a natural fracture system using finite element method. The second kind consists of simplified models based upon existing pseudo-3D models (Meyer and Bazan, 2011) or simplified rule-based analytical models for addressing the complex interactions between a created hydraulic fracture and a natural fracture system (Kresse et al., 2011). In the third kind, the authors who have developed and applied the models in capturing the fundamental hydro-mechanical behavior of hydraulic fracturing in naturally fractured reservoir. Damjanac et al. (2010) presented the results of hydraulic fracture modeling in a naturally fractured reservoir with a discrete element model (DEM). In the model, they highlighted the impact of fluid compressibility on hydraulic fracture geometry (a very compressible fluid created a more complex fracture geometry). Further, Nagel et al. (2011a, 2011b) have presented specific modeling results of hydraulic fracture simulations using DEM tools.

In shale fracturing, one of the challenges that influence the stimulation and productivity predication is the heterogeneity of reservoirs. Firstly, in mesoscopic scale, the rock matrix is composed of different kinds of minerals, crystal grains, pores, miro-cracks, etc. Also, the natural fractures are of great development in natural reservoirs from the macroscopic perspective. The results of MMHF used in shale stimulation showed that a large number of fractures were propagating simultaneously or sequentially. The naturally fractured formations under hydraulic pressure exhibit a unique feature: the flow and transport behavior within developing fractures are dramatically different from those in rocks with existing fractures under the same loading. The permeability of rocks with existing fractures does not change, but it can change dramatically due to damage evolution in fracturing rocks. The influences of damage on the variation of permeability as well as the original nature of the existing fractures in reservoirs are critical to the shear stimulation of natural fractures. Another major problem in characterizing the hydraulic behavior of reservoirs concerns the irregular flow paths that depend on the mechanical heterogeneity of the formations. In working with heterogeneous rocks, a key factor is to determine the specific data that are needed to ascertain the effect of heterogeneity on the complicated flow paths in fracturing formations. To solve the coupled flow-damage problems, Tang et al. (2002) proposed a flow-stress-damage (FSD) coupling model by taking the growth of existing fractures and the formation of new fractures into account. This FSD model can be used to trace the development of fractures and the associated fluid flow, and to simulate the overall response of rock masses arising from the fracture process under hydraulic and boundary loadings. This FSD model is different from the finite element modeling and distinct element modeling. The most unique feature of this code, which makes it totally different from other kind of numerical codes is that it can simulate the whole shear stimulation process of pre-existing fractures and their interaction with hydraulic fractures in hydraulic fracturing (Tang et al., 2002; Wang et al., 2009, 2011).

The focus of this work is on the numerical investigation of the shear stimulation effect during hydraulic fracturing in different discrete fracture networks (DFNs) using a FSD coupled model (RFPA-Flow). This study focuses on how the natural fracture networks influence the effect of hydraulic fracturing, but not the interaction between hydraulic fractures and pre-existing natural fractures. A series of comparative simulations were performed in an initial attempt towards understanding how reservoirs response to fluid injection by some of the geomechanical parameters and to operational variables such as injection rate. The established simulations consider various *in-situ* parameters, including the DFN orientation within the stress field, the *in-situ* stress ratio, the friction angle of the natural fractures, and an operational parameter such as injection rate.

The results of the study provide a further quantitative evaluation of hydraulic fracturing. They also provide a sensitivity investigation on the critical parameters affecting shale gas production, and help understand and optimize hydraulic fracture stimulations in naturally fractured reservoirs.

2. Numerical approach

RFPA-Flow code developed by Tang et al. (2002), is a numerical simulation tool using finite element analysis to analyze the progressive failure of heterogeneous, permeable rock. In the model, the coupled effects of flow, stress and damage on the extension of existing/new fractures and the permeability change due to damage evolution of the rocks were addressed. This coupled flow, stress and damage (FSD) model in RFPA-Flow has been validated in the previous publications (Yang et al., 2001; Tang et al., 2002; Wang et al., 2009). By extending Biot's theory to include the effects of stress on permeability, the basic formations of the analysis are:

equilibrium equation

$$\frac{\partial \sigma_{ij}}{\partial x_{ij}} + \rho X_j = 0, \quad (i, j = 1, 2, 3); \tag{1}$$

strain-displacement equation

$$\varepsilon_{ij}=\frac{1}{2}\left(\mu_{i,j}+\mu_{j,i}\right),\quad \varepsilon_v=\varepsilon_{11}+\varepsilon_{22}+\varepsilon_{33};\tag{2}$$

constitutive equation

$$\sigma'_{ij}=\sigma_{ij}-\alpha p\delta_{ij}=\lambda\delta_{ij}\varepsilon_v+2G\varepsilon_{ij};\tag{3}$$

seepage equation

$$k\nabla^2 p=\frac{1}{Q}\frac{\partial p}{\partial t}-\alpha\frac{\partial\varepsilon_v}{\partial t};\tag{4}$$

coupling equation

$$k\left(\sigma,p\right)=\xi k_0\exp\left[-\beta\left(\frac{\sigma_{ii}/3-p}{H}\right)\right].\tag{5}$$

Eqs. (1)–(4) are based on Biot's theory of consolidation (Biot, 1941), and eq. (5) represents the effect of stress on permeability, which is introduced to describe the dependency of permeability on stress and damage, and the relationship between permeability and stress is assumed to follow a negative exponential function.

When the stress of the element satisfies the strength criterion (such as the Coulomb criterion), the element begins to fail. In elastic damage mechanics, the elastic modulus of the element may degrade gradually along with damage progresses, and the elastic modulus of the damaged element is defined as below:

$$E=\left(1-D\right)E_0,\tag{6}$$

where D is the damage variable, E and E_0 are elasticity modulus of the damaged and the undamaged material, respectively.

When the tensile stress in an element reaches its tensile strength f_t', this is

$$\sigma'_3\le -f'_t.\tag{7}$$

The damage variable was described by Tang et al. (2002) as:

$$D=\begin{cases}0, & \overline{\varepsilon}\le\varepsilon_{\text{to}},\\ 1-\dfrac{f_{\text{tr}}}{E_0\overline{\varepsilon}}, & \varepsilon_{\text{to}}\le\overline{\varepsilon}\le\varepsilon_{\text{tu}},\\ 1, & \overline{\varepsilon}>\varepsilon_{\text{tu}},\end{cases}\tag{8}$$

where f_{tr} is the residual tensile strength of the element, and $\overline{\varepsilon}$ is equivalent principal strain of the element, ε_{to} is the strain at the elastic limit, or threshold strain, and ε_{tu} is the ultimate tensile strain of the element at which the element would be completely damaged. In this case the permeability can be described as:

$$k=\begin{cases}k_0\exp\left[-\beta\left(\sigma'_3-\alpha p\right)\right], & D=0,\\ \xi k_0\exp\left[-\beta\left(\sigma'_3-\alpha p\right)\right], & 0<D\le 1,\end{cases}\tag{9}$$

where ξ (ξ>1) is the damage factor of permeability, which reflects the damage-induced permeability increase (Tang et al. 2002). The value of ξ can be obtained from experimental tests (Thallak et al., 1991; Noghabai, 1999).

In the model, both tensile and shear failure modes are considered. An element is considered to have failed in the tension mode when its minor principal stress exceeds the tensile strength of the element, as described by eq. (6), and have failed in shear mode when the compressive or shear stress has satisfied Mohr-Coulumb failure criterion given by Tang et al. (2002):

$$F=\sigma'_1-\sigma'_3\frac{1+\sin\phi'}{1-\sin\phi'}\ge f'_c,\tag{10}$$

where σ'_1 is the major effective principal stress, σ'_3 is the minor effective principal stress, ϕ' is the minor effective angle of friction, f'_t is the tensile failure strength of the element, and f'_c is the compressive failure strength of the element. The damage factor under uniaxial compression is described as:

$$D=\begin{cases}0, & \overline{\varepsilon}<\varepsilon_{\text{cu}},\\ 1-\dfrac{f'_{\text{cr}}}{E_0\varepsilon}, & \overline{\varepsilon}\ge\varepsilon_{\text{co}},\end{cases}\tag{11}$$

where f'_{cr} is the residual compressive strength, ε_{cu} is the ultimate compressive strain of the element at which the element would be completely damaged (Tang et al., 2002). In this case, the permeability can be described by

$$k=\begin{cases}k_0\exp\left[-\beta\left(\sigma'_1-\alpha p\right)\right], & D=0,\\ \xi k_0\exp\left[-\beta\left(\sigma'_1-\alpha p\right)\right], & D>0.\end{cases}\tag{12}$$

In RFPA-Flow, the specified loading is applied to the specimen incrementally in a quasi-static manner. Coupled seepage and stress analyses are performed. At each loading increment, the seepage and stress equations of the elements are solved and a coupling analysis is performed. The stress conditions of each element are then examined for failure before the next load increment is applied. If some elements are damaged in a particular step, their reduced elastic modulus and increased permeability at each stress or strain level is calculated using the above damage variable D as well as eq. (5). Then the calculation is restarted under the current boundary and loading conditions to redistribute the stresses in the specimen until no new damage occurs. Finally, the external load (or displacement) is increased and is used as input for the next step of the analysis. Therefore, the progressive failure process of a brittle material subjected to gradually increasing static loading can be simulated. A user-friendly pre- and post-processor is integrated in RFPA-Flow to prepare the input data and display the numerical results.

There are two features distinguishing RFPA-Flow from other numerical approaches: (1) by introducing heterogeneity of rock properties into the model, the RFPA-Flow code

can simulate non-linear deformation of a quasi-brittle behavior with an ideal brittle constitutive law for the local material; (2) by introducing a reduction of material parameters after element failure, the RFPA code can simulate strain-softening and discontinuous mechanics problems in a continuum mechanics mode. For heterogeneity, the material properties (failure-strength σ_c and elastic modulus E_c) for elements are randomly distributed throughout the model by following a Weiibull distribution:

$$\varphi = \frac{m}{\sigma_0}\left(\frac{\sigma}{\sigma_0}\right)^{m-1} \exp\left[-\left(\frac{\sigma}{\sigma_0}\right)^{m}\right], \quad (13)$$

where σ is the element strength and σ_0 is the mean strength of the elements for the specimen, and φ is the probability that a material property variable. For an elastic modulus, E, the same distribution is used. m is defined as the homogeneity index of the rock (Tang et al., 2002). According to the definition, a larger m implies a more homogeneous material and *vice versa*.

3. Models

In this paper, RFPA-Flow was used to evaluate the effect of hydraulic fracturing, so to qualitative evaluate the effect of such parameters on hydraulic fracturing; the model responses are compared in terms of a series of indices that were evaluated during hydraulic fracturing. These indices include: (1) the DFN orientation within the stress field; (2) stress ratio, which is defined here as the increase in SH_{max} over the SH_{min}; (3) the friction angle of the natural fractures, and (4) the injection rate to the naturally fractured formations. The key part of the numerical model is the DFN. The DFN realizations were constructed statistically according to prescribed parameter distributions. Olson (2008) has provided an extensive discussion and photo assembly of formation outcrops, the photo was shown in Figure 1 and papers reported by Olson (2003, 2004) helped inspiring the DFN formulation. Figure 1 illustrates a cliff outcrop with joint spacing approximately proportional to bed thickness of sandstone in Marcellus Shale Formation. The geological structure of the outcrop is composed of two joint sets; they are beddings and cross joints. According to the research results (Sagy and Reches, 2006), mean or medium joint spacing in layered rocks is often linearly related to layer thickness, and it was suggested that the saturation intensity (D_s=h/d) for realistic geological cases converges to the range of D_s=0.75–3.0 (i.e., d/h=1/3–4/3). In the model, the injection fluid went through a vertical wellbore in the center of the model, and the increasing injection fluid was imposed on the wellbore at constant rate. The natural fractures were intersected with the wellbore. Figure 2 is the geometry and model setup. The whole model is composed of 40000 (200×200) identical square elements with dimension of 400 m×400 m. The diameter of the injection hole is 15 m. Four kinds of DFN configurations were created for the simulations, each DFN model consisted of two fracture sets, which were called bedding joint and cross joint. The bedding joint had a spacing of 25 m with normal distribution, STD, of 1 m. The cross joint had a spacing of 30 m with normal distribution and STD, of 3 m. A series of simulations were conducted to evaluate the influence of the various parameters on the effectiveness of hydraulic fracturing and the natural fracture shearing caused by an injection wellbore. The simulation cases evaluated three stress ratios (*SR*=0.02, 0.1, and 0.2), three internal friction angle of fracture (*IFA*=10°, 20°, and 30°), four DFN orientations (*OR*=0°, 15°, 30°, and 45°), and three injection rates (*IR*=0.1, 0.3, and 0.5 MPa). The input material mechanical parameters for the numerical models are based on the work of Gale et al. (2008), the main parameters used for hydraulic fracturing is shown in Table 1. For all the simulations, the slick-water-frac treatment is selected during the simulations, fluid rheology is 1 cp.

4. Results of numerical modeling

4.1 General observations

The results of the base case model (*OR*=45°, *SR*=0.02, *IR*=0.5 MPa, *IFA*=10°) was simulated and showed the

Table 1 Input material mechanical parameters for the numerical models

Index	Rock matrix	DFN
Homogeneity index (m)	2	3
Elastic modulus (E_0) (GPa)	56	10
Poisson's ratio (v)	0.2	0.3
Internal friction angle (φ) (°)	45	10, 20, 30
Compressive strength (σ_c) (MPa)	260	23, 28, 34
Tensile strength (σ_t) (MPa)	26	2.3, 2.8, 3.4
Coefficient of residual strength	0.1	0.1
Permeability coefficient (k_0) (md)	0.0004	0.009
Coupling coefficient (β)	0.01	0.01
Coefficient of pore-water pressure (a)	0.6	0.6

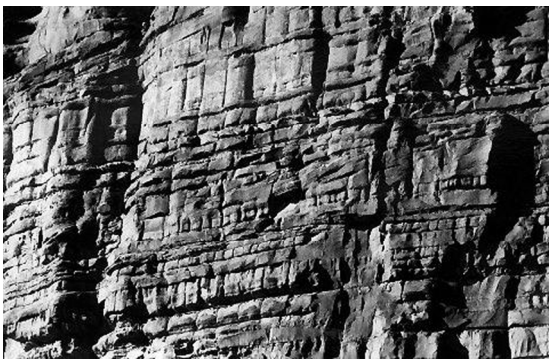

Figure 1 The geological outcrop of sandstone in Marcellus Shale Formation (after Olson, 2008).

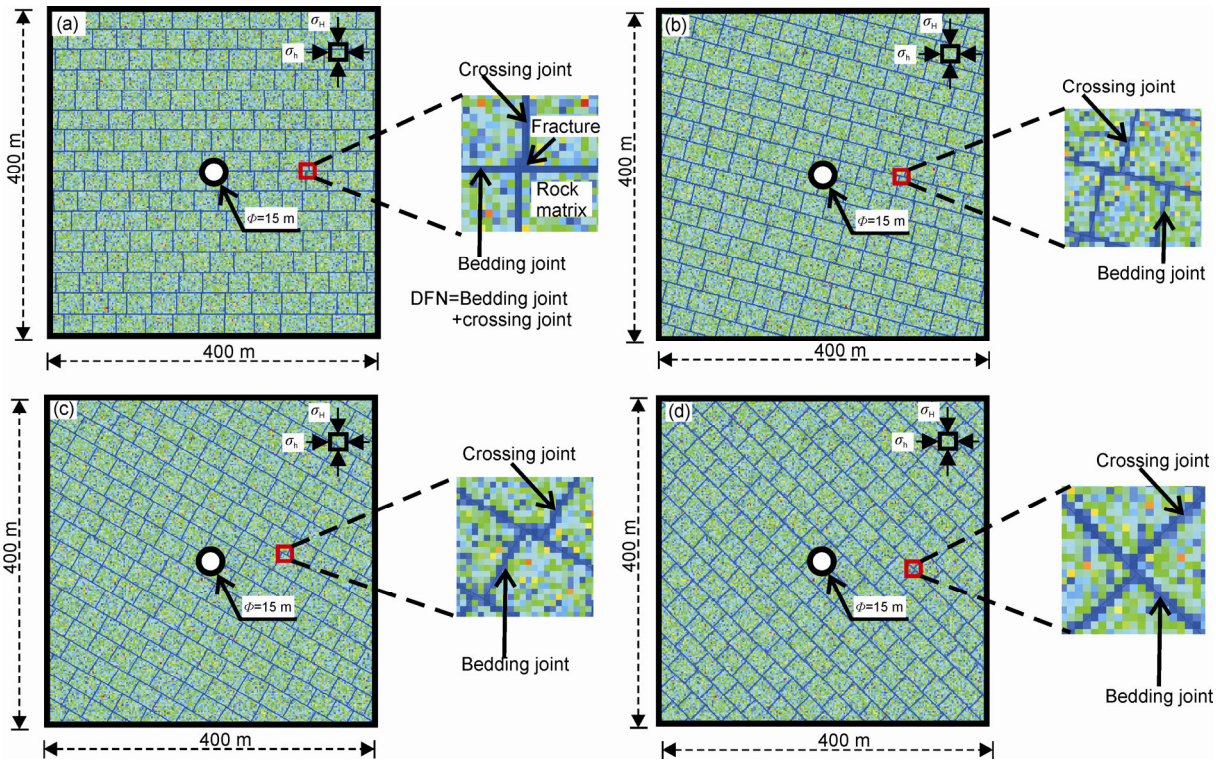

Figure 2 The geometry and model setup. The DFN orientation was 0° (a), 15° (b), 30° (c), and 45° (d), respectively.

progressive shear stimulated process of DFN. Figure 3 shows the pore pressure distribution characteristics due to increasing hydraulic pressure. In these figures, different colors indicate relative magnitude of the pore water pressure. With the increasing hydraulic pressure in the wellbore, pore pressure propagates to a much large portion of the DFN, local DFN elements begin to damage and become reactive. The simulation results show that the hydraulic fracturing process can be divided into three stages. (1) Stress accumulation stage. In this stage, it does not show any damage and

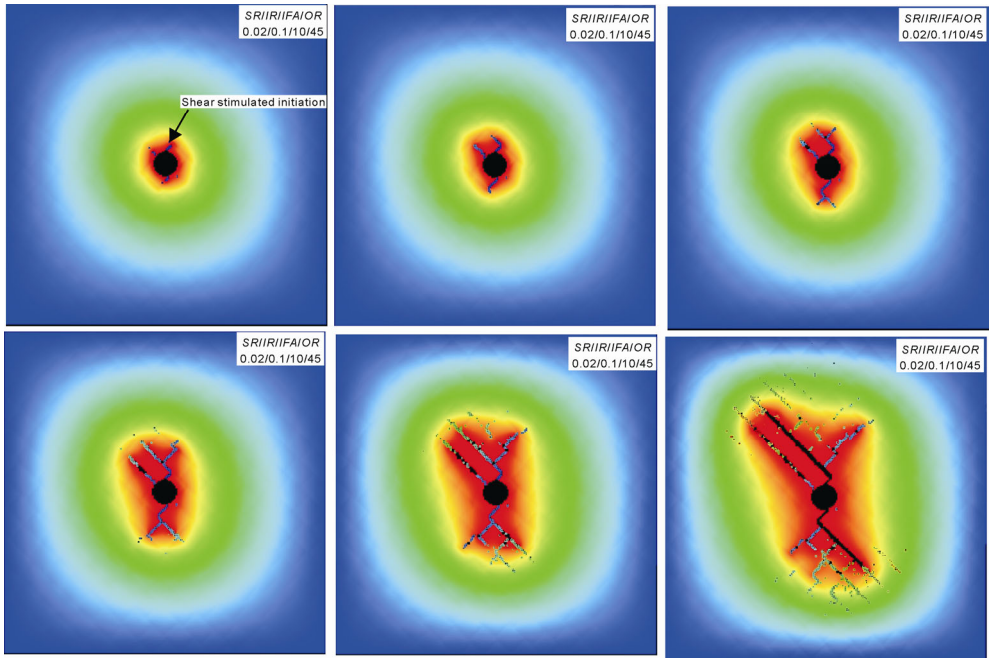

Figure 3 Numerically simulated the shear stimulation process of the base case with DFN orientation 45°, stress ratio 0.02, injection rate 0.1 MPa and internal friction angle 10°. Color shadow indicates relative magnitude of the pore pressure field.

failure element, but as the pore pressure increases gradually, the stress accumulates around the wellbore and forms a high minimum principal stress zone. (2) Crack steady propagation stage. When the pore pressure around the wellbore reaches to a certain value, local DFN elements begin to damage and they are stimulated by shearing. (3) Crack unsteady propagation stage. In this stage, the hydraulic pressure does not appear to add up, but the propagation of natural fractures becomes faster and faster, lots of fractures are connected in the end, and now, the shear stimulated DFN area reaches to the maximum. With RFPA-Flow approach, number of the failed elements and the associated energy can be recorded, which can be treated as indicators of AE activates that accompany with hydraulic fracturing. The plot of the variations of diameter (vertical and horizontal) and AE counts versus the fluid pressure, as shown in Figure 4, the similar conclusion can also be drawn. The constant rate of diameter increase suggests a stable fracture propagation until step 46 (point a). At point b (step 58), the borehole diameter elongation and the AE rate increase drastically until the pressure reaches its peak level (breakdown pressure). This indicates the unstable propagation without increasing water pressure. The result is consistent with the analysis published by Cipolla et al. (2009a).

In the following analysis, in order to qualitatively evaluate the effect of hydraulic fracturing, the model responses are compared in terms of a series of indices that were evaluated during the injection. These indices include: (1) injection pressure, defined as the fluid pressure that was injected into the wellbore. (2) DFN affected surface area, defined as the surface area of the DFN that has experienced a fluid pressure increase due to injection (Figure 5). This surface area corresponds to the strong leak-off region; the pore pressure in this region is greater than in other regions. (3) DFN shear stimulated length, defined as the total shear reactive length of nature fractures which appear to damage and open during fluid injection (Figure 5). (4) DFN shear stimulated area, defined as the area of natural fractures that

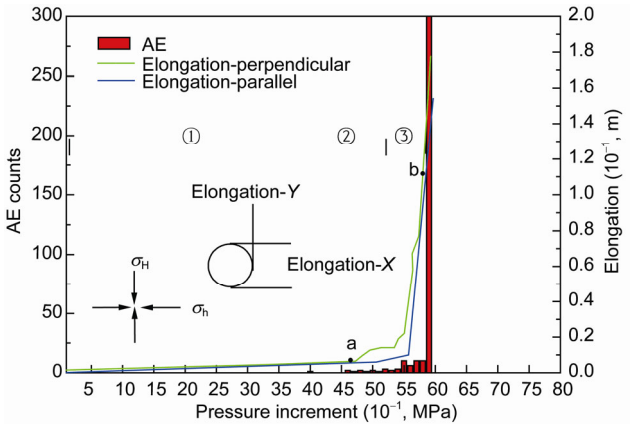

Figure 4 The relationship of AE counts, wellbore diameter and injection pressure. ① stress accumulation stage; ② crack steady propagation stage; ③ crack unsteady propagation stage.

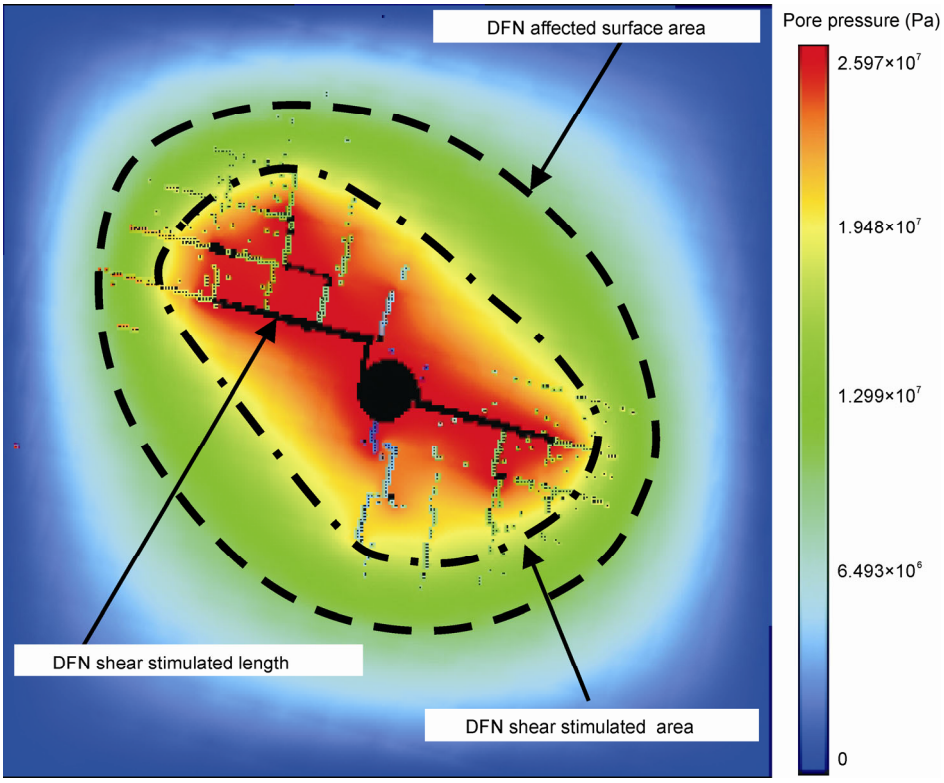

Figure 5 Description of the indices used to evaluated the effect of hydraulic fracturing.

have experienced shear slippage (Figure 5).

4.2 Effect of the stress ratio

The *in-situ* stress contrasts obviously have the most significant effect on fracture height growth. The importance of *in-situ* field stress was recognized early in 1961 (Perkins and Kern, 1961) and has been extensively studied in modeling (Simonson et al., 1978; Voegele et al., 1983; Palmer and Luiskutty, 1985), mineback tests (Warpinski et al., 1982), and numerous laboratory experiments. But few reports about how the stress contrast affects the shear stimulation were reported. Stress ratio (which is defined as the increase in SH_{max} over SH_{min} here) also plays an important role in the generation of natural fracture shear stimulation. Therefore, the primary interest in simulating the sensitivity of stress ratio is to obtain a better understanding of how output is affected by it. Figure 6 shows the results of DFN shear stimulated morphology with DFN orientation equals to 0°, 15°, 30°, and 45°, respectively. The results indicated that as the stress ratio increases, the shear failure pattern is different. Shear stimulated zone gradually parallels to the maximum horizontal principal *in-situ* stress with increasing of stress ratio. Taking the DFN orientation equals to 0° for example, when SR=0.02, the direction of shear stimulated zone is about 45° to the SH_{max}; when SR=0.1, the included angle is about 75°; and when SR=0.2, the included angle is about parallel to the maximum *in-situ* stress. Results of Figure 6 suggest that, the DFN stimulated surface area is decreasing with the increase of stress ratio.

As stated above, the fractures were reactive when the injection pressure reaches to a certain point. Before this point, no fractures occur. And when the injection pressure reaches to the breakdown pressure, the cracks propagate unsteady until failure of the model. Therefore, we only analyze the DFN characteristics quantitatively at the crack unsteady propagation stage. Figure 7 shows the effect of elevated stress ratio, history of quantitative indices. As there are no precise criteria for defining the interaction area, a criterion based on fracture pressure change was employed in this work. The area having a pore pressure increase of 15 MPa above the initial pore pressure was considered as the DFN shear stimulated area, which surrounds the shear stimulated natural fractures. The plot of the DFN shear stimulated area in different injection steps shows that *in-situ* stress has a significant influence on the fracture reactive area. The results also suggest that natural fracture orientation within the stress field has a consequential influence on the shear of the fractures during a simulation. Figure 8 shows that the DFN shear stimulated length follows a similar trend to the DFN shear stimulated area. These figures show that as the stress ratio increases, the natural fractures tend to initiate and propagate much faster. There appears to be less disconnected shear region at fracture intersections. However, under the same condition of SR=0.2 for DFN orientation equal to 45°, the shear stimulated area and length are greater than the other three cases.

To compare the DFN shear stimulated area and length during hydraulic fracturing, it can be seen that the *in-situ* stress field has a strong influence on the shear stimulation of natural fractures (Figure 8). When the formations are under the isotropic far-field stress, large regions of shear fractures would be reactive easily, and *vice versa*.

4.3 Effect of the friction angle

The objective of this study is to evaluate the effect of the friction angle of DFN on responses to fluid injection during hydraulic fracturing. From Figure 6, it is clearly observed that massive shear stimulated regions cannot be clearly seen in field cases. One important reason for this, also a reason that is commonly ignored, is that shearing occurs when there is a change in the initiating force (the net pressure of the hydraulic fracture) relative to the resident force (the strength of the rock or fracture). Figure 9 shows how the increasing of friction angle influences the DFN shear stimulated area.

Figure 10 shows the effect of elevated friction angle, history of quantitative indices. The net pressure in each model was the same; the changes of stress for the simulations were also the same. Consequently, the sole cause of the difference in shear among those simulations is the increase in internal friction angle. The plot of the DFN shear stimulated area versus injection step shows that shear stimulated area decreases with increasing of friction angle. This result highlights that, even if the simulation treatment was identified between the two wells, and even if the natural fracture system was exactly the same, if the strength parameters of the natural fracture system (either friction angle or cohesion) change, then the formation shear behavior, as well as the effectiveness of the stimulation will differ.

Figure 11 plots the DFN shear stimulated length versus friction angle following a similar trend to the DFN shear stimulated area. These figures indicate that as the friction angle increases, the natural fractures tend to initiate, propagate more slowly. The shear strength of the fracture increases with increasing of friction angle, the shear length with the natural fracture system is small with high friction angle.

4.4 Effect of DFN orientation

As stated above, the designed angle of orientation includes 0°, 15°, 30°, and 45°, respectively. DFN is the most uncertain part of the model. Therefore, the primary interest in simulating the sensitivity of DFN orientation is to obtain a better understanding of how output is affected by it. Actually, in Section 3.2 (Figure 6), it has indicated that DFN orientation has a strong influence on the stimulated region. Figure 12 shows quantitative comparison of the DFN shear

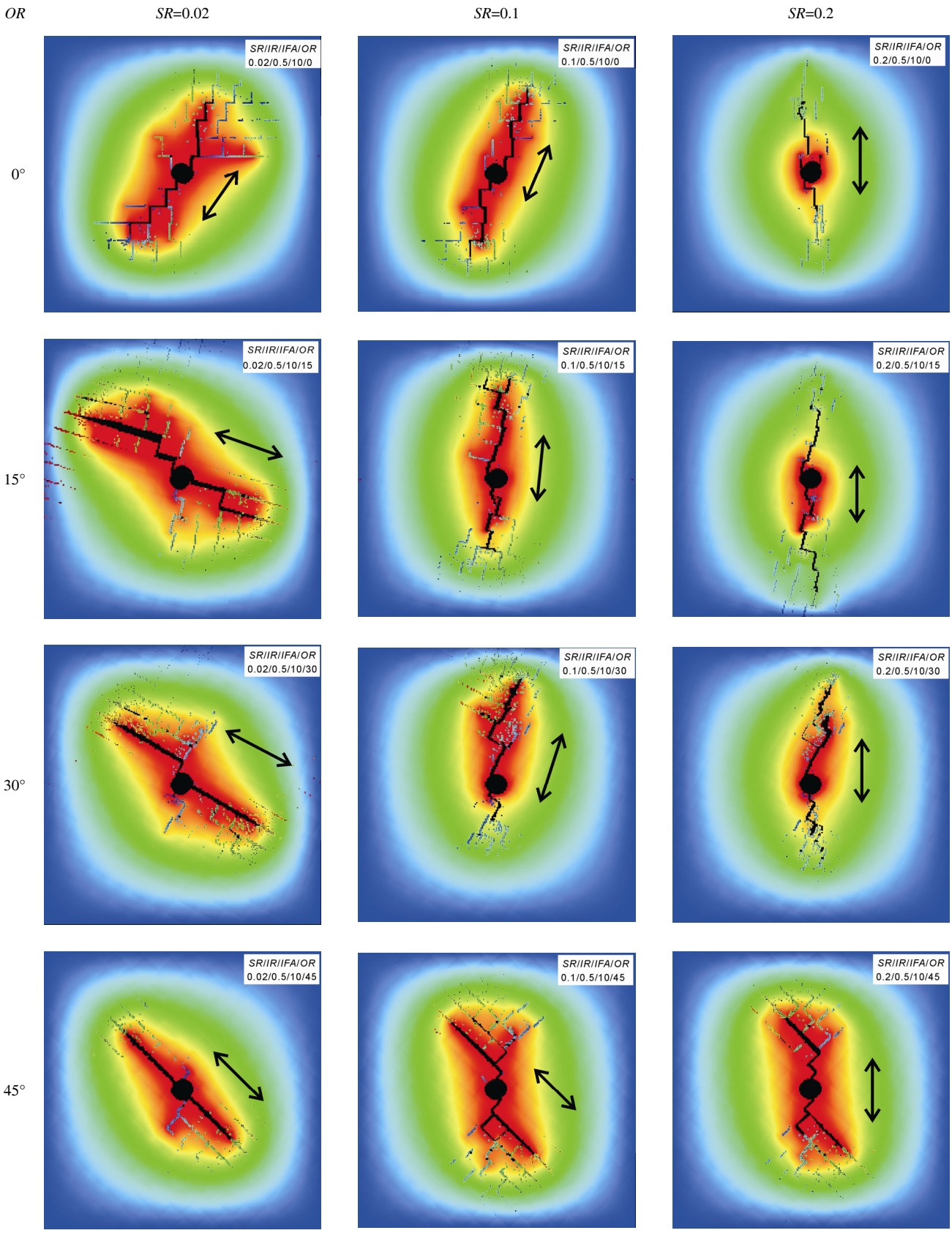

Figure 6 The effect of the stress ratio on the morphology of shear stimulated zone. *IR*=0.5 MPa, *IFA*=10°, and DFN orientation is 0°, 15°, 30°, and 45°, respectively. Color shadow indicates relative magnitude of the pore pressure field.

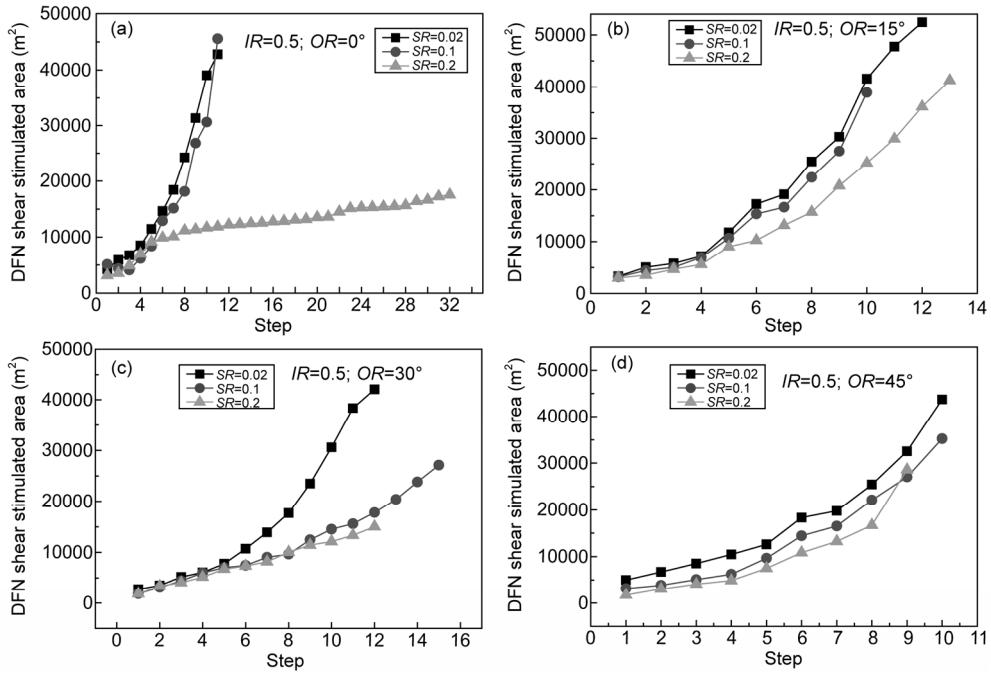

Figure 7 The relationships between DFN shear stimulated area and injection step with stress ratio 0.02, 0.1 and 0.2, respectively. (a)–(d) The injection rate is 0.5 MPa and the DFN orientation is 0°, 15°, 30°, and 45°, respectively.

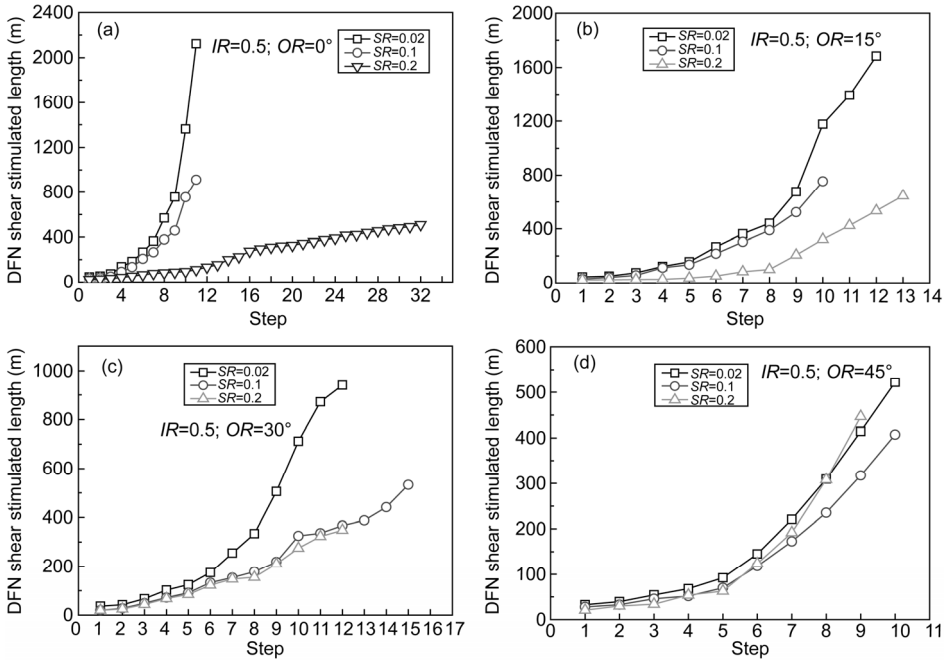

Figure 8 The relationships between DFN shear stimulated length and injection step with stress ratio 0.02, 0.1 and 0.2, respectively. (a)–(d) The injection rate is 0.5 MPa; DFN orientation equals to 0°, 15°, 30°, and 45°, respectively.

stimulated area and length between different DFN orientations. The history of injection step at wellbore (Figure 12(a)) shows that as the DFN orientation increases, the stimulated area deceases. Figure 12(b), which shows the DFN shear stimulated length, indicates that the shear stimulated length at smaller DFN orientation is evident than bigger orientation. These observations can be better interpreted by evaluating the pore pressure contours shown in Figure 6. These pressure contours indicate that for the studied DFN configurations, in lower bedding geology structure, the shear stimulation of natural fractures are the most evident compared to the other circumstances. Sayers and Le Calvez (2010) reported that fracture complexity is thought to be enhanced when pre-existing fractures are oriented at an angle to the maximum

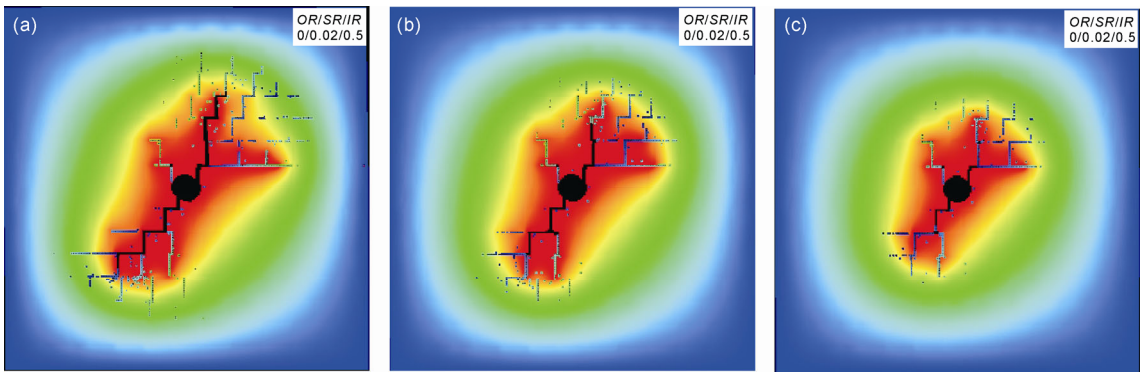

Figure 9 Comparison of natural fracture shear for *IFA*=5° (a), 20° (b), and 30° (c). In this case, *OR*=0°, *SR*=0.02 and *IR*=0.5 MPa.

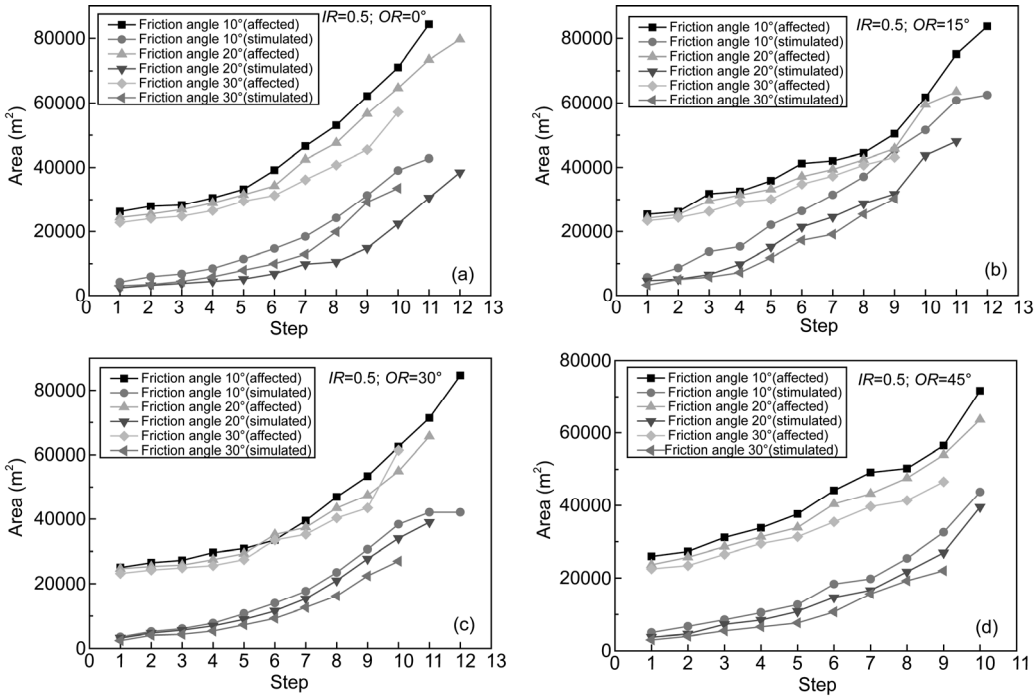

Figure 10 The responses of DFN shear stimulated area to friction angle with different orientation at *IR*=0.5 MPa. (a)–(d) DFN orientation equals to 0°, 15°, 30°, and 45°, respectively.

stress direction, or when both horizontal stresses and horizontal stress anisotropy are low, because these combinations of stress and natural fractures allow fractures in multiple orientations to be stimulated. In this section, we have also drawn the similar conclusions which prove the reliability of our simulations.

4.5 Effect of injection rate

The injection rate and injection pressure along with the viscosity of the injected fluid are the operational parameters that can be used to effectively design hydraulic fracturing and DFN stimulation. Currently, slick-water fluid with minimum viscosity has been evolved to increase the formation-face contact of fracture system in a very located area of reservoirs by opening natural fractures (King, 2010; Kresse et al., 2011). In this paper, the water-frac is used to stimulate the natural fractures. In this section, it is evaluated how the injection rate (pressure increment rate) affects the reservoir stimulation.

Firstly, the considered range of injection rates is such that it covers injection pressure below the breakdown pressure. Figure 13(a) shows the relationship between DFN affected surface area and injection step. Figure 13(b) plots the DFN affected surface area against injection pressure, the injected pressure is the same for the different simulations. Figure 13(a) shows that for a similar injection step, higher injection rates result in a greater DFN affected area. However, in Figure 13(b), the plot of the DFN affected area versus injected pressure shows a reverse trend that is observed for the DFN affected area versus injection step. That is because, for similar injected pressure, greater injection rates result in

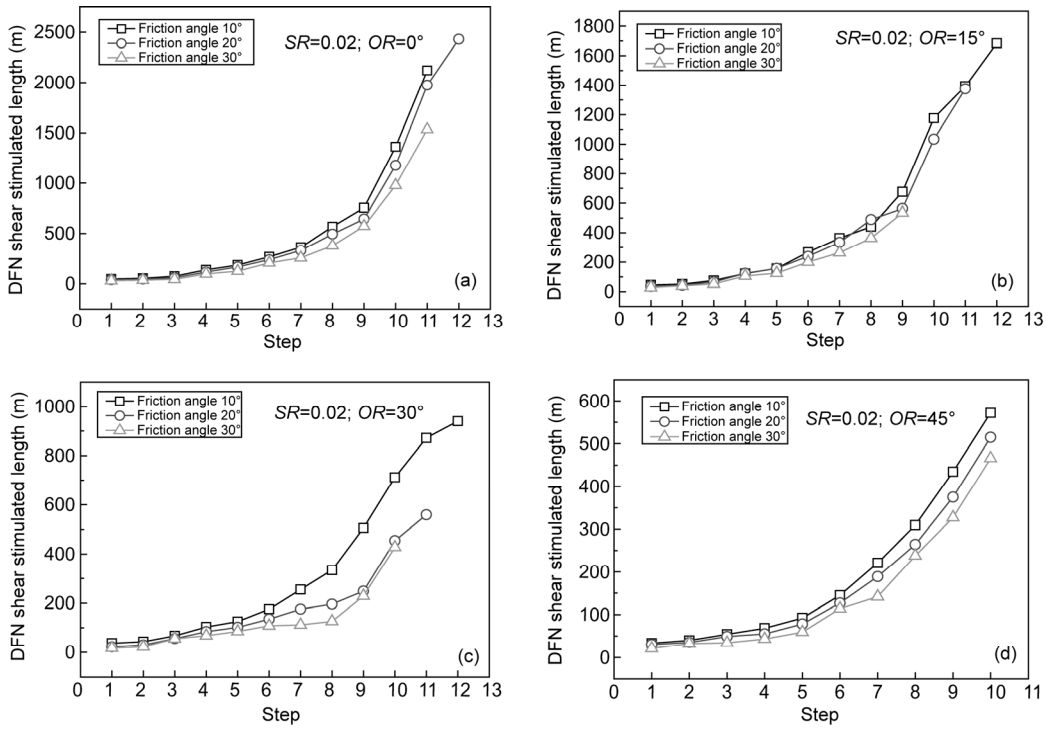

Figure 11 The responses of DFN shear stimulated length to internal friction angle with different orientation at *IR*=0.5 MPa. (a)–(d) The DFN orientation equals to 0°, 15°, 30°, and 45°, respectively.

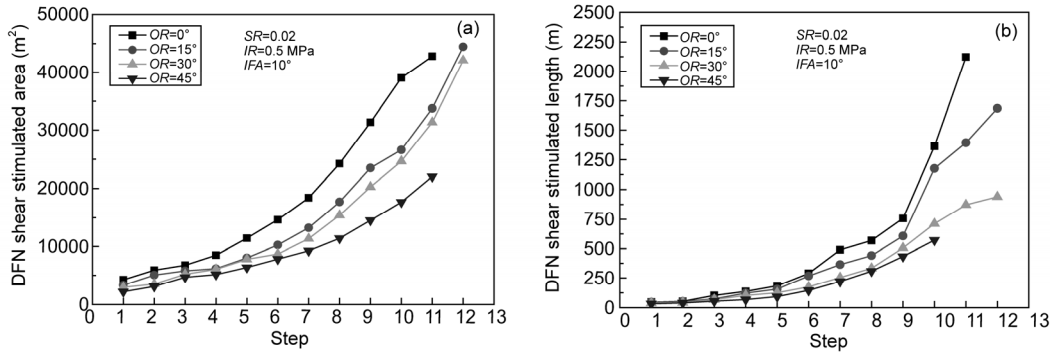

Figure 12 Effect of DFN orientation on the shear stimulated area and length when the injection pressure reaches to breakdown pressure. In this case, *SR*=0.02, *IR*=0.5, and internal friction angle of DFN is 10°.

smaller fluid leak-off into the formations. For a smaller injection rate, the time required to inject a similar pressure is much longer, the injection fluid leak-off the formation to a large extent. Thus, during this longer time, the pressure front can propagate to a larger distance from the injection well. Figure 13(c) and (d) show that higher injection rates can result in a greater DFN stimulated area and DFN stimulated length, respectively.

Secondly, when the injection pressure reaches to the breakdown pressure, it does not need to inject pressure further, the shear stimulated fractures propagate continually. As shown in Figure 14, the DFN shear stimulated area and length increase gradually, all the fluid is pumped into the fracture system, which results in the damage and reactivation of sealed natural fractures. The pore water pressure drives the fractures to propagate, and form a large stimulated area. Also, the injection rate significantly affects the leak-off ratio for natural fractured formations; the hydraulic fracturing effectiveness increases with fluid leaking off into the model. When the injection pressure reaches to the breakdown pressure, the higher injection pressure is applied, the better hydraulic fracturing effectiveness can be obtained.

5. Conclusions

In this work, we have numerically investigated the shear stimulation effect in naturally furcated formations. A series of simulations were conducted to explore the influence of some key parameters on the hydraulic fracturing. This designed

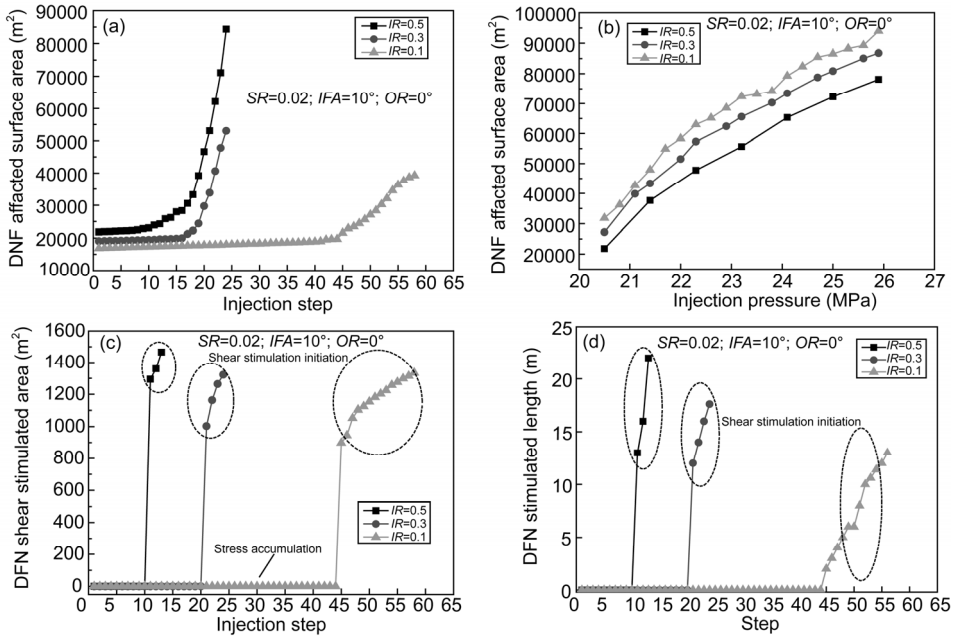

Figure 13 Effect of injection rate on the DFN affected area and shear stimulated area before injection pressure reaches to the breakdown pressure. (a), (b) Correspond to the injection pressure below breakdown pressure; (c), (d) correspond to the injection pressure equals to breakdown pressure.

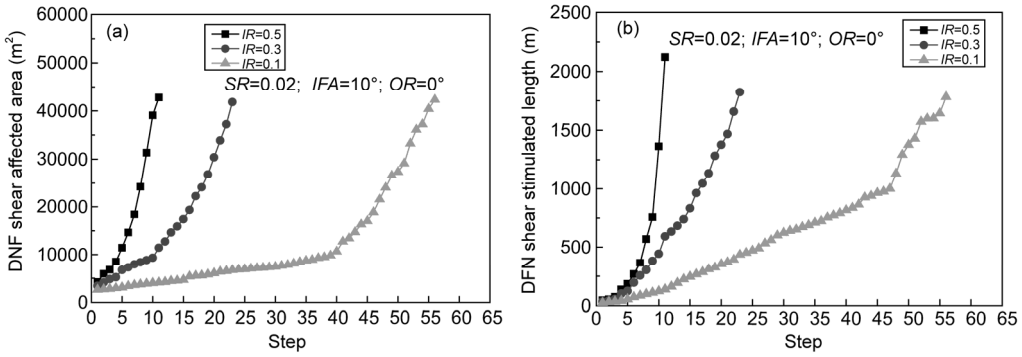

Figure 14 Effect of injection rate on the DFN affected area and shear stimulated area when injection pressure equals to the breakdown pressure.

numerical work cannot be substituted for the hydraulic fracturing design tools, but it can help us to understand and grasp the effects of hydraulic fracturing with some important geomechanical parameters and the operational parameters.

From the sensitivity study in this paper, the following conclusions can be drawn.

(1) For the simulations performed, the stress ratio has the most significant influence on the reaction of natural fractures. The stress ratio was shown to alter both the extent and morphology of the sheared natural fractures. As stress ratio increases, a greater volume of formation experiences stimulation along the natural fractures. More importantly, with increasing stress ratio, natural shear becomes more directional (dominantly parallel to the SH_{max} direction), with limited shear along orthogonal fractures. In isotropic stress field, the fracturing effect is the best. With the increase of stress ratio, the shear stimulated area decreases, and the hydraulic fracturing effect becomes poorer.

(2) The degree of fracture shear is directly related to the fracture friction angle. Fracture angle is a critical parameter to shear stimulation and thus to well production.

(3) When the DFN orientation equals to 0°, the effectiveness of shear stimulation is evident. With the increase of DFN orientation, the simulation effect is not desired. This highlights the importance of understanding the orientation of the fracture network with the *in-situ* stress field.

(4) The shear of fractures is linked to the MS events; the shear region within the natural fracture system is strongly related to the geomechanical parameters of shales.

(5) For the considered case of DFN model, because the fractures open against a lower stress, the lower the horizontal stress anisotropy is, the more the DFN is stimulated. This result is partially pre-determined by the assumption of non-shear dilatancy in the base case model. Indeed, the stress anisotropy would enhance the shear dilatancy of natural

fractures. More sensitivity simulations are recommended to better understand relative contributions of these two counteracting effects.

(6) Injection rate plays a major role in the shear of natural fracture system. When injection pressure is smaller than the breakdown pressure, smaller injection rate results in a greater affected surface area; and greater injection rates result in a greater stimulated surface area. When injection pressure reaches the breakdown pressure, the fractures propagate faster without increasing the injection pressure at all, and greater injection rates result in greater stimulated area and length.

Acknowledgements *We thank the reviewers for their helpful and constructive suggestions and comments. This work was supported by the National Natural Science Foundation of China (Grant Nos. 41227901, 41330643 & 41502294), China Postdoctoral Science Foundation Funded Project (Grant No. 2015M571118), and the Strategic Priority Research Program of the Chinese Academy of Sciences (Grant Nos. XDB10030000, XDB10030300 & XDB10050400).*

References

Biot M A. 1941. General theory of three-dimensional consolidation. J Appl Phys, 12: 155–64

Chong K K, Grieser W V, Passman A, Tamayo C, Modeland N, Burke B E. 2010. A Completions Guide Book to Shale-Play Development: A Review of Successful Approaches Towards Shale-Play Stimulation in the Last Two Decades. In: Canadian Unconventional Resources and International Petroleum Conference, 19–21 October, Calgary, Alberta, Canada. Paper CSUG/SPE 133874

Cipolla C L, Lolon E P, Erdie J C, Tathed V S. 2009a. Modeling well performance in shale-gas reservoirs. In: Presentation at the SPE/EAGE Reservoir Characterization and Simulation Conference. Abu Dhabi, UAE, October 19–21

Cipolla C L, Lolon E P, Mayerhofer M J. 2009b. Reservoir modeling and production evaluation in shale-gas reservoirs. In: The International Petroleum Technology Conference. Doha, Qatar, 7–9 December

Damjanac B, Gil I, Pierce M, Sanchez M, Mclennan J. 2010. A new approach to hydraulic fracturing modeling in naturally fractured reservoirs. In: The 44th US Rock Mechanics Symposium, Salt Lake City, Utah, USA, 27–30 June. Paper ARMA 10-400

Gale J F W, Holder J. 2008. Natural fractures in the Barnett shale: Constraints on spatial organization and tensile strength with implications for hydraulic fracture treatment in shale-gas reservoirs. In: The 42nd US Rock Mechanics Symposium (USRMS). San Francisco, CA, June 29–July 2

Jeffrey R G, Zhang X, Bunger A P. 2010. Hydraulic fracturing of naturally fractured reservoirs. In: Proceedings of the 35th Workshop on Geothermal Reservoir Engineering. Stanford, California, USA, 1–3 February

King G E. 2010. Thirty years of gas shale fracturing: What have we learned? In: SPE Annual Technical Conference and Exhibition. Florence, Italy, 19–22 September. Paper SPE 133456

Kresse O, Cohen C, Weng X, Gu H G, Wu R T. 2011. Numerical modeling of hydraulic fracturing in naturally fractured formations. In: The 45th US Rock Mechanics Symposium. San Francisco, California, USA, 26–29 June. Paper ARMA 11-363

Mayerhofer M J, Lolon E P, Warpinski N R, Cipolla C L, Walster D W, Rightmire C R. 2010. What is stimulated reservoir volume? SPE Prod Oper, 25: 89–98

Mayerhofer M J, Lolon E P, Youngblood J E, Heinze J R. 2006. Integration of microseismic fracture mapping results with numerical fracture network production modeling in the Barnett shale. In: The SPE Annual Technical Conference and Exhibition. San Antonio, Texas, September 24–27

Meyer B R, Bazan L W. 2011. A discrete fracture network model for hydraulically induced fractures—Theory, parametric and case studies. In: SPE Hydraulic Fracturing Technology Conference and Exhibition. The Woodlands, Texas, USA, 24–26 January. Paper SPE 140514

Nagel N, Gil I, Sanchez-Nagel M. 2011a. Simulating hydraulic fracturing in real fractured rock—Overcoming the limits of pseudo 3D models. In: SPE Hydraulic Fracturing Technology Conference and Exhibition. The Woodlands, Texas, USA, 24–26 January. Paper SPE 140480

Nagel N, Sanchez-Nagel M. 2011b. Stress shadowing and microseismic events: A numerical evaluation. In: SPE Annual Technical Conference and Exhibition. Denver, Colorado, USA, 30 October–2 November. SPE 152192. Paper SPE 147363

Nassir M, Settari A, Wan R. 2010. Modeling shear dominated hydraulic fracturing as a coupled fluid-solid interaction. In: International Oil and Gas Conference and Exhibition. Beijing, China, 8–10 June. Paper SPE 131736

Noghabai K. 1999. Discrete versus smeared versus element-embedded crack models on ring problem. J Eng Mech, 125: 307–315

Olson J E. 2003. Sublinear scaling of fracture aperture versus length: An exception to the rule? J Geophys Res, 108: 1–11

Olson J E. 2004. Predicting fracture swarms—The influence of subcritical crack growth and the crack-tip process zone on joint spacing in rock. Geol Soc Lon Spec Pub, 231: 73–88

Olson J E. 2008. Spatial organization of natural fractures: A geomechanics approach. Nat Fract Pattern Dev. 2008–2010

Palmer I D, Luiskutty C T. 1985. A model of the hydraulic fracturing process for elongated vertical fractures and comparisons of results with other models. In: SPE/DOE Low Permeability Gas Reservoirs Symposium. Denver, Colorado, 19–22 May. Paper SPE 13864

Palmer I, Moschovidis Z. 2010. New method to diagnose and improve shale gas completions. In: SPE Annual Technical Conference and Exhibition. Florence, Italy, 19–22 September. Paper SPE 134669

Perkins T K, Kern L R. 1961. Widths of hydraulic fractures. J Petrol Technol, 13: 937–949

Rahman M M, Aghighi A A, Rahman S S. 2009. Interaction between induced hydraulic fracture and pre-existing natural fracture in a poroelastic environment: effect of pore pressure change and the orientation of a natural fractures. In: Asia Pacific Oil and Gas Conference & Exhibition. Jakarta, Indonesia, 4–6 August. Paper SPE 122574

Sagy A, Reches Z. 2006. Joint intensity in layered rocks: The unsaturated, saturated, supersaturated, and clustered classes. Isr J Earth Sci, 55: 33–42

Sayers C, Le Calvez J. 2010. Characterization of microseismic data in gas shales using the radius of Gyration tensor. SEG Expanded Abstract

Simonson E R, Abou-Sayed A S, Clifton J J. 1978. Containment of Massive Hydraulic Fractures. SPE J, 18: 27–32

Tang C A, Tham L G, Lee P K K. 2002. Coupled analysis of flow, stress and damage (FSD) in rock failure. Int J Rock Mech Min Sci, 39: 477–489

Thallak S, Rothenbury L, Dusseault M. 1991. Simulation of multiple hydraulic fractures in a discrete element system. In: Roegiers J C, ed. Rock Mechanics as a Multidisciplinary Science, Proceedings of the 32nd US Symposium. Rotterdam: Balkema. 271–280

Voegele M D, Abou-Sayed A S, Jones A H. 1983. Optimization of stimulation design through the use of *in-situ* stress determination. J Petrol Tech, 35: 1071–1081

Wang S Y, Sloan S W, Liu H Y. 2011. Numerical simulation of the rock fragmentation process induced by two drill bits subjected to static and dynamic (impact) loading. Rock Mech Rock Eng, 44: 317–336

Wang S Y, Sun L, Au A S K, Yang T H, Tang C A. 2009. 2D-numerical analysis of hydraulic fracturing in heterogeneous geo-materials. Constr Build Mater, 23: 2196–2206

Warpinski N R, Finley S J, Vollendorf W C, Obrien M, Eshom E. 1982. The interface test series: An *in-situ* study of factors affecting the containment of hydraulic fractures. Sandia National Laboratories Report, SAND, 2381–2408

Warpinski N R, Mayerhofer M J, Vincent M C, Cipolla C L, Lolon E. 2009. Stimulating unconventional reservoirs: maximizing network growth while optimizing fracture conductivity. J Can Petrol Technol, 48: 39–51

Yang T H, Tang C A, Zhu W C, Feng Q Y. 2001. Coupling analysis of seepage and stress in rock failure process (in Chinese). Chin J Rock Soil Eng, 23: 489–493